Temperature programming for isothermal desorption rate measurements

Cite as: Journal of Vacuum Science & Technology A **10**, 3507 (1992); https://doi.org/10.1116/1.577810
Submitted: 21 February 1992 . Accepted: 10 July 1992 . Published Online: 04 June 1998

Michael A. DeAngelis and A. Brad Anton

Temperature programming for isothermal desorption rate measurements

Michael A. DeAngelis and A. Brad Anton
School of Chemical Engineering, Cornell University, Ithaca, New York 14853-5201

(Received 21 February 1992; accepted 10 July 1992)

We describe a digital feedforward/feedback controller for the implementation of rapid changes in the temperature of a small, resistively heated metal adsorbent in ultrahigh vacuum. The feedforward loop is based on a second-order model of the system's thermal response, modified by inclusion of a time delay to account for the characteristic time for heat conduction in the adsorbent, and the feedback loop includes proportional and derivative actions. These features allow the temperature of a nickel single crystal, 10 mm diameter and 1 mm thick, to be increased 80 K within approximately 4 s without overshoot, after which desorption rates can be measured at constant surface temperature with a mass spectrometer. The performance of the temperature controller and the advantages of isothermal data collection and analysis are demonstrated with CO desorption from Ni(110), for which the functional dependence of the rate on surface coverage at constant temperature identifies clearly the participation of a mobile precursor state in the desorption process.

I. INTRODUCTION

Accurate measurement of rate parameters, e.g., the reaction order or the activation energy, is essential for identifying mechanistic features of any surface reaction. For a desorption or surface reaction that yields gaseous products, mass spectrometry provides a very sensitive technique for measuring the time- or temperature-dependent evolution of desorbing molecules for kinetics analysis. Measurements based on this approach are now standard components of nearly every published investigation of reactive surface chemistry in ultrahigh vacuum (UHV).

A typical experiment involves preparation of an adsorbed layer at a temperature sufficiently low that the reaction rate is negligible, after which the temperature of the sample is ramped linearly in time, i.e., $T(t) = T_0 + \beta t$, where T_0 is the initial temperature, β is the heating rate, and t is time, and the partial pressures of desorbing gases are monitored with the mass spectrometer. This approach has been given several names in the literature,[1] but for the purposes of our discussion, we will refer to it as "ramp temperature-programmed desorption" (ramp-TPD). When the pumping time is small compared to the characteristic time over which the reaction proceeds, as is usually the case in UHV, the partial pressure of the reaction product measured by the mass spectrometer is proportional to the desorption rate.[1] The shape of rate vs temperature curve generated in this manner is related to the functional dependence of the rate on surface coverage, i.e., the reaction order,[2] and many methods have been proposed for extracting rate parameters, i.e., activation energies and preexponential factors,[3] from the data.

Although the simplicity of implementing the linear temperature ramp makes this approach appealing, data collected in this manner are often not uniquely interpretable, since the rate coefficient and reactant coverage vary simultaneously as the experiment proceeds. To appreciate this, consider the rate expression for simple, one-step desorption:

$$r(t,\vartheta) = \nu \exp\left(\frac{-E}{RT}\right)\vartheta^n, \tag{1}$$

where r is the desorption rate, T is the adsorbent temperature, ν is the preexponential factor, E is the activation energy, ϑ is the surface coverage of adsorbed reactant, and n is the order of the reaction (typically, $n = 1$ or $n = 2$). The sensitivity of the ramp-TPD line shape to the rate parameters in Eq. (1) can be determined from the total derivative of the rate with respect to temperature, evaluated with $dT/dt = \beta$:

$$\frac{dr}{dT} = r\left(\frac{E}{RT^2} - \frac{nr}{\beta\vartheta}\right). \tag{2}$$

One observes that the line shape function involves a balance between two contributions, the first of which dominates on the low temperature side of the TPD peak as the signal rises, and the second of which dominates on the high temperature side as the signal falls. Only at the leading edge of the low temperature side, where the rate and signal intensity approach zero, does the line shape show a simple dependence on a rate parameter:[4]

$$\lim_{r\to 0}\left(\frac{d[\ln(r)]}{d(1/RT)}\right) = -E. \tag{3}$$

Otherwise, the line shape function convolutes the features of the rate function together in a complex fashion, and this problem is exacerbated when the rate parameters change with coverage or a single-step rate function is inappropriate. Although they did not state their arguments in exactly these terms, Soler and Garcia addressed the same issues when they demonstrated that ramp-TPD data published and analyzed by other investigators can be fit equally well with numerous kinetic models.[5]

Other problems can arise from the experimental implementation of the linear temperature ramp. In some cases preparation of the adsorbed layer at a low temperature may "trap" it in a nonequilibrium configuration that has insufficient time to relax during the ramp, yielding desorp-

 0734-2101/92/063507-10$01.00

tion from nonequilibrium configurations.[6] Another concern is temperature nonuniformity in the sample during transient heating, particularly when it is a metal, supported in the typical fashion by thin wires connecting its edges to a cooling reservoir and heated resistively by passing electrical current through the wires. If the resistivity of the current path through the sample is negligibly small compared to that of the support wires, as is usually the case, all heat is generated in the wires and conducts into the adsorbent. The resulting temperature gradient maintains a constant temperature difference between the outer edges and the center of the sample during the ramp, the magnitude of which is approximately $\Delta T \approx \beta l^2/2\alpha$, where l and α are the sample's half-width and thermal diffusivity, respectively.[7] For example, heating a nickel single crystal with a half-width of $l \approx 5$ mm at $\beta = 30$ K/s gives $\Delta T \approx 15$ K, which is comparable to the width of typical ramp-TPD peaks and can lead to significant errors in line shape analysis.

Many of these difficulties can be circumvented if the desorption measurement is performed instead with the adsorbent temperature held constant. For a sample supported by heating wires as described above, the temperature variation at steady state is due only to radiative heat exchange between it and the surroundings, since heat generation in the support wires has the effect of thermally isolating the sample from the cooling reservoir. For this case the one-dimensional energy balance reduces to

$$\frac{d^2T}{dx^2} - \frac{\epsilon\sigma}{\kappa\gamma}(T^4 - T_s^4) = 0, \tag{4}$$

where ϵ is the emissivity, σ is the Stefan–Boltzmann constant, κ is the thermal conductivity, γ is the ratio of volume to surface area for the sample, T is its temperature, and T_s is the temperature of the surrounding chamber.[8] Solving this with $T = T_e$ at the edges ($x = \pm l$), with $dT/dx = 0$ at the center ($x = 0$), and with the approximation $T^4 - T_s^4 \approx \langle \Delta T^3 \rangle (T - T_s)$, where the quantity $\langle \Delta T^3 \rangle = (T + T_s)(T^2 + T_s^2)$ is assumed constant, one obtains

$$\frac{T(x) - T_s}{T_e - T_s} = \frac{\cosh(\delta x)}{\cosh(\delta)}, \tag{5}$$

where $\delta = l(\epsilon\sigma\langle \Delta T^3 \rangle/\kappa\gamma)^{1/2}$. With $\epsilon \approx 0.12$ and $\kappa \approx 90$ W/m K (for nickel), $\gamma \approx 3$ mm, $T_e \approx 800$ K, and $T_s \approx 300$ K, the temperature varies across the sample by less than 0.01 K, thus is uniform to an excellent approximation.

Note that a uniform temperature will not be possible if the adsorbent is instead heated by radiation or electron bombardment from a hot filament and cooled by conduction to the sample holder. Although heat can be added to the sample more uniformly in this arrangement, heat removal by conduction to the sample holder at the support points is generally nonuniform, producing a significant temperature gradient even at steady state. The resulting temperature profile can introduce errors in isothermal data analysis, analogous to the problem for ramp-TPD with direct, resistive heating alluded to above.[7] For isothermal data acquisition and analysis, the uniform temperature distribution afforded by resistive heating is preferred.

When the adsorbent temperature is constant and uniform, the reaction rate is a function of coverage and time only, and simple expressions like Eq. (1) can be separated and integrated analytically for comparison to isothermal desorption line shapes. Alternatively, the measured rate can be converted by integration with respect to time to rate vs coverage for algebraic comparison to the predictions of kinetic models of the desorption process. Also, the isothermal line shapes can be analyzed with the classical techniques of chemical kinetics (method of half lives, etc.[9]), and their shapes are more clearly related to reaction order than are the shapes of ramp-TPD line shapes. As will be demonstrated in Sec. IV, the net effect is more certain identification of reaction mechanisms and more accurate and precise estimations of rate parameters.

Two approaches can be envisaged for isothermal data collection. One possibility is to prepare the adsorbed layer by exposure of the surface to reactants to attain equilibrium at the temperature of desorption, after which the reactant flux is shut off and desorption proceeds, as in modulated molecular beam relaxation spectroscopy[10] or in novel applications of time-resolved electron energy loss spectroscopy.[11] This offers the advantage that desorption occurs from an adsorbed layer initially at equilibrium. However, technical difficulties associated with providing temporal control of the reactant flux and pumping speed sufficient to eliminate background effects can complicate this approach. A second possibility is to prepare the adsorbed layer at a low temperature T_1, as in traditional ramp-TPD measurements, and to program the temperature to change rapidly to a higher temperature T_2, where the reaction rate is appreciable and data are collected. In subsequent discussion we will refer to this latter method as "step-TPD" to distinguish it from ramp-TPD. The second approach is by comparison much simpler, and it affords the added advantage that the adsorbed layer can be characterized by other experimental techniques at low temperature, prior to the onset of reaction. Nonequilibrium effects may be introduced by the rapid temperature change,[6] but one expects these to be rarely important, particularly if the measurement begins with the surface saturated.

When implementing step-TPD, a paramount concern is the amount of time required to complete the temperature change, since this ultimately delimits the flexibility and dynamic range of the measurement. In order to identify the correct rate function with confidence, it is necessary that the isothermal rate is measured over several increments of the characteristic reaction time, which can be assumed approximately equal to $1/k(T_2)$, where $k(T_2)$ is the rate constant at the higher temperature. As the temperature increases from T_1 during the step, desorption begins unavoidably before T_2 is reached and isothermal data collection can commence. When the temperature transient is slow, desorption during the transient depletes the surface coverage, decreasing the length of time and range of coverage over which the isothermal rate can be measured. This may leave insufficient structure in the isothermal data to identify uniquely a kinetic model for the desorption process. Because of this consideration, the largest reaction rate

constant that can be measured, and therefore the upper limit of the technique's dynamic range, is limited by the step time. The issue we address in this paper is generation of the most rapid temperature change possible with resistive heating.

Several investigations in the literature have included data collected with the step-TPD approach,[12] but the dynamic range in these measurements has been severely limited by the time required to achieve the temperature change, typically more than 10 s. We suspect the limiting factor has been the troublesome overshoot and oscillations that occur when traditional feedback schemes are used for temperature control. The cause and possible remedies for the overshoot problem have not been addressed in this context. We describe herein an optimal control scheme that allows the temperature step to be accomplished in the shortest time possible, limited only by the system's ability to add and remove heat from the adsorbent. The performance of the controller and the utility of isothermal rate measurements is demonstrated with partial results of an investigation of CO desorption from Ni(110).[13]

II. APPARATUS

The experiments were performed in a two-chamber system with a base pressure of 2×10^{-10} mbar. One chamber contains the sample manipulator, a sputter ion gun, facilities for LEED and AES, and a directional gas doser,[14] and the other houses a quadrupole mass spectrometer with provisions for ion counting (Vacuum Generators SX-200). The main chamber is evacuated with a 400 ℓ/s ion pump and a liquid nitrogen-cooled titanium sublimation pump, and the mass spectrometer chamber is evacuated with a 170 ℓ/s turbo pump and a sublimation pump, positioned to give high pumping speed near the ionizer. The two chambers are connected through a 3 mm orifice that provides line-of-sight from the ionizer to the sample.

The sample, a disk approximately 10 mm diameter $\times$ 1 mm thick, is mounted to OFHC copper supports with 0.6 mm diameter $\times$ 5 mm long tantalum wires spot-welded to its edges, and the supports are bolted to the end of a 200 ml liquid nitrogen reservoir at the manipulator. Sapphire spacers are used between the copper supports and the reservoir to maintain electrical isolation without sacrificing thermal conductivity for cooling. The sample is heated resistively by passing current from a 50 A, 40 V programmable dc power supply (Hewlett-Packard 6269B) through the support wires and the sample. A chromel-alumel thermocouple for temperature measurement is spot-welded to the rear face of the sample near its center.

The adsorbent for the measurements reported here is a nickel single crystal, oriented, cut, and polished by standard techniques to expose a well-ordered (110) surface. It was cleaned by repeated cycles of argon bombardment, O_2 oxidation, H_2 reduction, and high temperature annealing. Surface order and cleanness were verified by LEED, by AES, and by the reproducibility of ramp-TPD curves for saturation exposures of CO or H_2.

The portion of the apparatus dedicated to control of the adsorbent's temperature is shown schematically in Fig. 1.

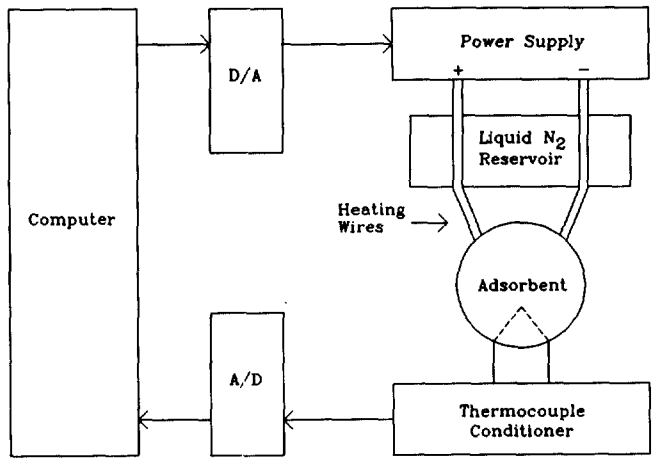

FIG. 1. Schematic diagram of the portion of the apparatus dedicated to control of the adsorbent's temperature.

A personal computer (AST 286) and interface board (MetraByte DAS-16G) serve as the control and data acquisition elements, determining the temperature of the sample with a thermocouple conditioner (Analog Devices 2B50A) and an analog-to-digital (A/D) converter, controlling the power supply that heats the sample with a D/A converter, and collecting the desorption signal from the ion multiplier of the mass spectrometer with a digital counter.

III. TEMPERATURE CONTROL ALGORITHM

Several basic principles of control strategy and implementation guide us in the choice of the controller configuration. The goal of our effort is to implement a smooth change in adsorbent temperature as rapidly as possible; i.e., the controller should maximize the heat input rate and minimize the response time. Traditional feedback control schemes are optimized to maintain the controlled variable at a steady value while load disturbances act on the system; however, they respond slowly to changes in the input setpoint, particularly in systems with time delays, because of their need to detect an error before acting. A *feedforward* scheme is instead preferred that uses a model of the controlled system to anticipate its response. When combined with a traditional feedback loop to correct for changing loads, the feedforward control strategy provides nearly optimal response to changes of the setpoint.[15]

This leads us to choose the feedforward/feedback control scheme depicted in the system block diagram of Fig. 2. The feedforward controller acts as a predictor for the system: Based on a model of the system's optimum response, i.e., the desired temperature program $T_a(t)$, it determines the power required by the system as a function of time, as quantified by the feedforward input $I_{FF}(t)$. The anticipated response is provided to the feedback loop as a setpoint program $T_{SP}(t)$, and the feedback controller acts upon the error $E(t) = T_{SP}(t) - T(t)$, i.e., the difference between the anticipated and measured temperature response, with proportional and derivative (PD) actions to correct the

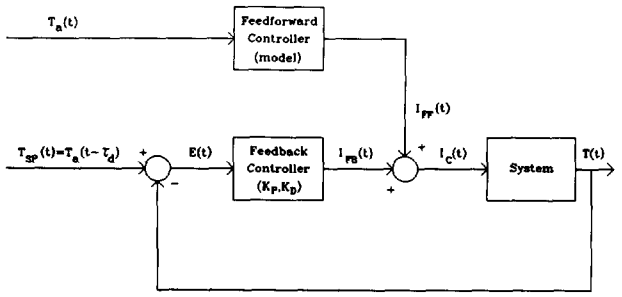

FIG. 2. Block diagram for feedforward/feedback control scheme. $T_a(t)$ is the ideal temperature program; $T_{SP}(t)$ is the setpoint, i.e., the anticipated temperature program including the time delay; $I_{FF}(t)$, $I_{FB}(t)$, and $I_C(t)$ are the feedforward, feedback, and combined controller outputs, respectively; $T(t)$ is the system's actual response, and $E(t) = T_{SP}(t) - T(t)$ is the error upon which the feedback controller acts, with K_P and K_D as the proportional and derivative gains, respectively.

controller's output for load disturbances and inadequacies in the feedforward model. Integral action, usually desired in the feedback loop to avoid constant setpoint offsets,[15] is not needed in this case because of the presence of the feedforward loop. A stringent requirement for effective operation of this scheme is an accurate feedforward model of the system's response.

The characteristics of the system's behavior required for feedforward control can be gleaned from its response to simple inputs. Figure 3 shows the result of an experiment designed to mimic the implementation of a rapid step change of $T(t)$. For $t<0$ simple feedback control holds the current near $i=14$ A to maintain a constant temperature of $T=200$ K. At time $t=0$, the feedback controller is deactivated, the current is suddenly increased to its maximum value $i=40$ A and held there for 2.0 s, and then it is quickly shut off. One observes that $T(t)$ remains at its initial value for about 0.5 s before it responds, then turns up, rises rapidly, and continues rising and peaks more than

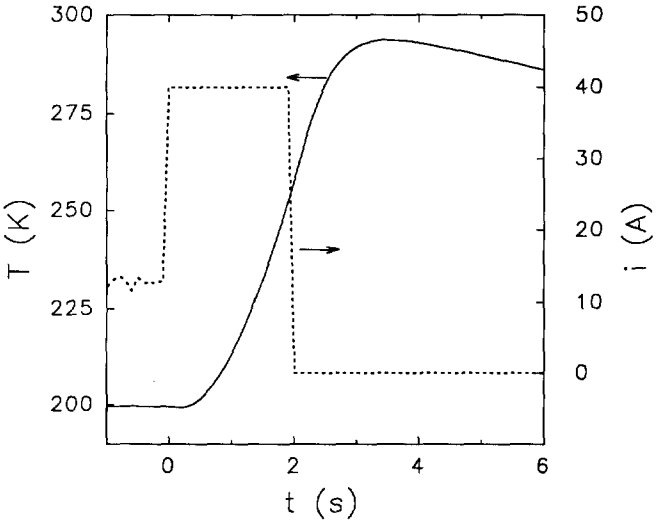

FIG. 3. Input current $I(t)$ and temperature response $T(t)$ for a simple experiment to characterize the system's behavior. The slow upturn of $T(t)$ suggests a second-order model is required, and the delayed response and overshoot indicate the presence of a time delay.

1 s *after* the current is shut off. The lack of an *immediate* relationship between current input and temperature response introduces a fundamental and severe instability, and this instability is manifested as overshoot and oscillations in response to rapid setpoint changes when traditional, feedback-only control schemes are implemented.[15]

We proceed to develop a mathematical model of the system that incorporates simplistic descriptions of the heat generation and conduction processes, involves few parameters, and yet successfully accounts for the behavior evident in Fig. 3. We assume initially that the entire adsorbent (a), the heating wires (w), and the cooling block (b) are described by uniform temperatures T_a, T_w, and T_b, respectively, and we assume that resistive heat generation due to dc current flow occurs only in the wires. The wires are connected to the sample and the cooling block with spotwelds, and we assume that the heat conduction rate from the wires through these contact points can be described by a conduction rate constant k. We do not include radiative heat transfer, since it is justifiably negligible in most circumstances (*vide supra*). Finally, the cooling block is assumed to have infinite mass, so the temperature T_b remains constant. These assumptions lead to the following set of coupled equations that describe the time evolution of the temperatures T_a and T_w:

$$m_a c_a \frac{dT_a}{dt} = k(T_w - T_a), \tag{6a}$$

$$m_w c_w \frac{dT_w}{dt} = [i(t)]^2 R - k(T_w - T_a) - k(T_w - T_b), \tag{6b}$$

where $m_a c_a$ and $m_w c_w$ are the products of mass and heat capacity for the adsorbent and wires, respectively; $i(t)$ is the time-dependent current supplied by the controller, and R is the net resistance of the two wires. Since heat is generated in the wires, T_w is much greater than T_a when T_a is increasing rapidly with time. For this reason, the value of R apparent during rapid heating is expected to differ significantly from that observed when T_a is held constant. This has important implications for the operation of the feedforward controller, as we will describe later.

At this point we recast and simplify Eqs. (6a) and (6b) to make direct connection with easily measured groups of parameters. First we define $I(t) = [i(t)/i_{max}]^2$ as a scaled variable that quantifies the relative amount of power input to the wires, where i_{max} is the maximum current that can be delivered.[16] The maximum is limited either by the capacity of the power supply that provides the heater current, or by the ability of the support wires to generate heat without melting. Also, we define $\kappa_a = k/m_a c_a$ and $\kappa_w = k/m_w c_w$ as the two inverse time constants for the coupled system, and $\rho = i_{max}^2 R/m_w c_w$ as the effective resistivity of the wires. In terms of these, Eqs. (6a) and (6b) are transformed to

$$\frac{dT_a}{dt} = \kappa_a(T_w - T_a), \tag{7a}$$

$$\frac{dT_w}{dt} = \rho I(t) - \kappa_w(T_w - T_a) - \kappa_w(T_w - T_b). \quad (7b)$$

Equations (7a) and (7b) can be combined into a single equation for d^2T_a/dt^2 that describes a second-order response for $T_a(t)$.

Since the mass of the adsorbent is much larger than that of the wires, $\kappa_w > \kappa_a$, and κ_a^{-1} is the long time constant that ultimately limits the response rate of the system. Clearly, "controllability" will benefit from minimizing m_a, the mass of the sample. Also, one can prove with simple scaling arguments that the solution to Eqs. (7a) and (7b) for $T_a(t)$ with $\kappa_w > \kappa_a$ includes a "boundary layer" of duration κ_w^{-1}. When the power input $\rho I(t)$ changes suddenly, $T_w(t)$ and $T_a(t)$ first respond over a time scale governed by κ_w^{-1}. This is evident in Fig. 3 as the slow turn of the temperature upward in response to the sudden increase of the current. After this time has passed, $dT_w/dt \approx 0$, and $T_a(t)$ follows approximately a first-order response curve described by

$$\frac{dT_a}{dt} \approx \frac{\kappa_a \rho I(t)}{2\kappa_w} - \frac{\kappa_a}{2}(T_a - T_b). \quad (8)$$

In this limit we recover Engstrom and Weinberg's first-order model for this problem,[16] which treats the wires and the adsorbent as a single entity and implicitly ignores the boundary layer. This is an adequate approximation for the steady-state behavior of the system and for situations where $I(t)$ changes slowly on the time scale of κ_w^{-1}, but it predicts a discontinuous change in dT_a/dt when $I(t)$ changes suddenly, in contrast to the response evident in Fig. 3. We find that this deficiency necessitates use of the complete second-order model for the feedforward controller, Eqs. (7a) and (7b).

Neither the second-order model nor the first-order simplification accounts for any time-dependent variation of the temperature *within* the adsorbent. The temperature within the adsorbent is *not* uniform during rapid heating because of the finite time required for heat to conduct from the edges, where the wires are attached, to the center, where $T_a(t)$ is measured.[7] This phenomenon is evident in Fig. 3 as the delay before $T_a(t)$ responds to the current increase and the overshoot of $T_a(t)$ after the current is shut off. An estimate of the characteristic time for heat conduction can be obtained from simple scaling arguments. To see this, consider the partial differential equation describing the combined temporal and spatial evolution of temperature in the disk-shaped adsorbent:[8]

$$\frac{\partial^2 T}{\partial r^2} + \frac{1}{r}\frac{\partial T}{\partial r} + \frac{1}{r^2}\frac{\partial^2 T}{\partial \vartheta^2} = \frac{1}{\alpha}\frac{\partial T}{\partial t}, \quad (9)$$

where r is radial distance from the disk's center, ϑ is azimuthal angle, and α is the thermal diffusivity of the adsorbent material. Since heat conducts from the edges to the center, the characteristic length scale is clearly r_0, the radius of the disk, but the temperature scale is arbitrary, since any scaling factor for T appears identically on both sides of the equation. Defining $\eta = r/r_0$, Eq. (9) can be rescaled to read

$$\frac{\partial^2 T}{\partial \eta^2} + \frac{1}{\eta}\frac{\partial T}{\partial \eta} + \frac{1}{\eta^2}\frac{\partial^2 T}{\partial \vartheta^2} = \tau\frac{\partial T}{\partial t}, \quad (10)$$

where $\tau = r_0^2/\alpha$. The form of Eq. (10) ensures that τ represents the characteristic time for heat conduction in this circumstance. Indeed, any solution to Eq. (10) obtained by separation-of-variables and including a boundary condition specified at $r = r_0$ will involve a series of time-dependent terms, the most slowly varying of which will have as its argument the quantity t/τ.[8] For the situation prevailing in our apparatus, $r_0 = 0.005$ m and $\alpha \approx 2\times10^{-5}$ m^2/s (for Ni), yielding $\tau = r_0^2/\alpha \approx 1$ s, in reasonable agreement with the delay apparent in the response curve of Fig. 3.

For the combined feedforward/feedback control scheme of Fig. 2 to operate effectively, the feedforward model described by Eqs. (7a) and (7b) must be modified to account for this phenomenon. The time for heat conduction in the adsorbent can be considered as a simple delay between the action induced at the edges, where heat is input, and the response at the center, where temperature is measured. Assuming this is an accurate representation of the system's behavior, an optimum feedforward current program $I_{FF}(t)$ can be identified that produces a desired temperature program $T_a(t)$ according to Eqs. (7a) and (7b), and the measured temperature should be the delayed response given by $T_a(t - \tau_d)$, where τ_d is the approximate delay time for heat conduction in the adsorbent. In the control loop $I_{FF}(t)$ is supplied by the feedforward controller; the delayed form of the optimum temperature program is used as the setpoint temperature $T_{SP}(t)$; and $E(t) = T_{SP}(t) - T(t)$, the difference between this and the actual system response, constitutes the error upon which the feedback loop acts, adding $I_{FB}(t)$ to the net controller output to correct for loads and disturbances. The net output of the combined feedforward/feedback controller is given by

$$I_C(t) = I_{FF}(t) + I_{FB}(t) = I_{FF}(t) + K_P E(t) + K_D\frac{dE(t)}{dt}, \quad (11)$$

where K_P and K_D are the proportional and derivative gains of the feedback control loop. Inclusion of the time delay in the setpoint temperature profile stabilizes the control loop, allowing large feedback gains to be used for load damping without introducing overshoot and oscillations when $I_{FF}(t)$ changes rapidly,[17] as is required for step-TPD.

A few simple measurements allow the five parameters in the feedforward model—T_b, κ_a, κ_w, ρ, and τ_d—to be estimated in any temperature range. It is important to recognize that the all the parameters are in principle functions of temperature due to the weak temperature dependencies of the contributing physical properties.[8] Therefore, a feedforward model based on constant values for the parameters can only be expected to predict the system's behavior accurately over the range where they have been measured. Once they are known as functions of temperature, it is a straightforward operation for the feedforward controller to choose values appropriate to the particular demands placed on it.

TABLE I. Typical feedforward model parameters and feedback gains.

Quantity	Magnitude	Description
T_b	80 K	cooling block temperature
κ_a	0.049 s^{-1}	$k/m_a c_a$, slow inverse time constant
κ_w	0.81 s^{-1}	$k/m_w c_w$, fast inverse time constant
ρ	1900 K/s	$i_{max}^2 R/m_w c_w$, effective wire resistivity for rapid heating ($i_{max}=40$ A)
κ_w/ρ	9.4–7.0$\times 10^{-4}$ K^{-1}	for steady-state control ($i_{max}=40$ A)
τ_d	0.40 s	delay time for heat conduction
τ_0	1.6 s	on time for maximum feedfoward output, $T_1=200$ K, $T_2=280$ K
K_P	0.040 K^{-1}	feedback proportional gain
K_D	0.040 s/K	feedback derivative gain

T_b can be recognized immediately as the temperature reached as $t\rightarrow\infty$ with $I(t)$ set to zero, and it can be assumed constant under all conditions. If the current is held constant at I_0 and the corresponding temperature T_0 is measured, the ratio κ_w/ρ is determined from the steady-state solution of Eq. (8):

$$I_0=\frac{\kappa_w}{\rho}(T_0-T_b). \tag{12}$$

This can be repeated for a range of temperatures to determine κ_w/ρ as a function of temperature for steady-state feedforward control. If the current is shut off at $t=0$ after the constant temperature T_0 is reached, the temperature decays after a few seconds according to the time-delayed solution of Eq. (8) with $I=0$:

$$\ln\left(\frac{T(t)-T_b}{T_0-T_b}\right)=-\frac{\kappa_a}{2}(t-\tau_d). \tag{13}$$

A cooling curve measured in this manner can be used to specify κ_a. The delay time τ_d can be estimated by visual inspection of the leading edge of a response curve like that of Fig. 3, and κ_w and a value of ρ appropriate for rapid heating can be determined from a two-parameter fit of the feedforward model to the shape of the response curve. As one might expect, the value of ρ determined in this way differs significantly from that identified in steady-state measurements according to Eq. (12), since the wire temperature T_w is on the order of 1000 K higher during rapid heating ($I=1$) than it is when T_a is held constant ($I\approx 0.1$).

Table I summarizes typical results of this analysis for our apparatus in the temperature range from 200 to 300 K. To protect the integrity of the heating wires, i_{max} is set conservatively to 40 A. T_b is approximately 80 K, and a cooling curve gives $\kappa_a=0.049$ s^{-1} in this range. Steady-state measurements show κ_w/ρ varying from 9.2×10^{-4} K^{-1} at $T_a=200$ K to 7.0×10^{-4} K^{-1} at $T_a=280$ K. The response curve of Fig. 3 identifies $\tau_d=0.40$ s, and a fit to its leading edge gives $\kappa_w=0.81$ s^{-1} and $\rho=1900$ K/s for rapid heating. In our experience the parameters κ_a, κ_w, and τ_d are nearly temperature invariant, but one must include the variation of ρ with temperature and operating conditions (rapid heating vs steady state) for satisfactory feedforward performance. Of course, all of these parameters must be quantified each time the sample is remounted or changed. Finally, empirical optimization of the feedback controller performance gives $K_P=0.040$ K^{-1} and $K_D=0.040$ s/K for the proportional and derivative gains, respectively, and these seem to work well for any temperature program in any range.

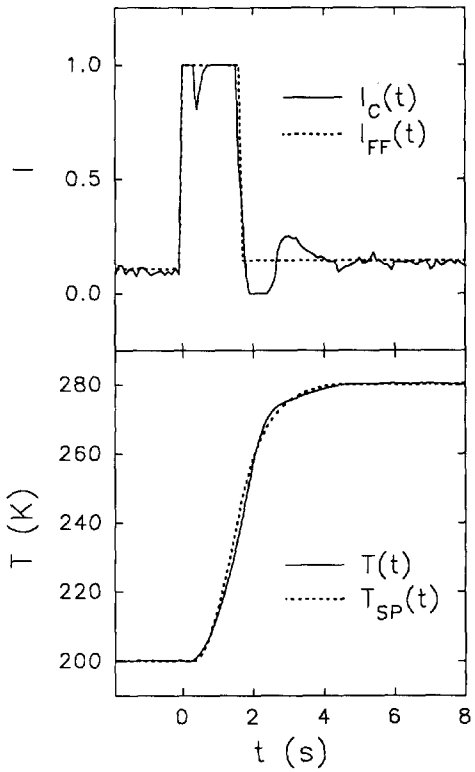

FIG. 4. Performance of the combined controller for a step from $T=200$ to 280 K. The top panel shows $I_{FF}(t)$, the output of the feedforward controller, and $I_C(t)$, that of the combined feedforward/feedback controller. The bottom panel compares $T(t)$, the actual temperature response, to $T_{SP}(t)$, the setpoint response predicted by the time-delayed model.

One may recognize intuitively that a nearly optimum feedforward output for performance of a rapid temperature change is like that shown as a dashed line for $I_{FF}(t)$ in the top panel of Fig. 4. For $t<0$ the feedforward controller supplies current $I_{FF}=I_1$ necessary to maintain the initial temperature T_1; at $t=0$ the output switches to $I_{FF}=1$ to deliver the maximum power to the adsorbent, causing its temperature to rise as fast as possible; and at $t=\tau_0$ the controller switches its output to $I_{FF}=I_2$, the current necessary to maintain $T=T_2$ for all time thereafter. Solving Eqs. (7a) and (7b) with this input for $I(t)$ and including the measured time delay τ_d gives the ideal response and setpoint $T_{SP}(t)$, detailed in the Appendix [Eqs. (A3)–(A5)] and shown schematically as a dashed line in the bottom panel of Fig. 4. With $T_1=200$ K and $T_2=280$ K for the example of Fig. 4 and the model parameters spec-

ified in Table I, the feedforward model gives $I_1 = 0.11$ and $I_2 = 0.14$. The "on-time" for maximum output of the feedforward controller is $\tau_0 = 1.6$ s [cf. Appendix, Eq. (A6)]. The solid lines in Fig. 4 show the actual controller output $I_C(t)$ (top panel) and the measured temperature response $T(t)$ (bottom panel) when this feedforward output and setpoint temperature profile are used with the combined feedforward/feedback controller. The deviation of $I_C(t)$ from $I_{FF}(t)$ shows clearly the substantial contribution of the feedback controller. One observes that the temperature response follows the setpoint very closely, and that the change from $T_1 = 200$ K to $T_2 = 280$ K is completed in approximately 4 s with effectively zero overshoot. This only a fraction of a second longer than the shortest time possible based on the apparent times for heat conduction and the maximum available heating rate in this temperature range, and it is sufficiently fast to allow isothermal decay curves to be collected for a maximum value of the desorption rate constant on the order of $k \approx 0.1\ s^{-1}$ at $T_2 = 280$ K.

Finally, we point out that this formalism can be easily extended to other temperature programs. For example, consider the problem of generating a linear temperature ramp. The output for the feedforward controller in this case is obtained by solving Eqs. (7a) and (7b) for $I(t)$ with $T_a(t) = T_0 + \beta t$ and $dT_a/dt = \beta$. For $t < 0$, $I_{FF} = I_0$ to maintain the constant initial temperature T_0, and for $t > 0$ one obtains

$$I_{FF}(t) = \frac{\beta}{\rho}\left(1 + \frac{2\kappa_w}{\kappa_a}\right) + \frac{\kappa_w}{\rho}(T_0 - T_b) + \frac{\kappa_w \beta t}{\rho}. \quad (14)$$

The setpoint for use by the feedback loop is the time-delayed form of the ramp, i.e., for $0 < t < \tau_d$, $T_{SP}(t) = T_0$, and for $t > \tau_d$, $T_{SP}(t) = T_0 + \beta(t - \tau_d)$. The constant ρ is simply updated by the computer to account for its temperature variation as the ramp proceeds.

Engstrom and Weinberg have shown that the kinetics of surface reactions can be incisively investigated via sinusoidal modulation of the adsorbent's temperature.[18] For this case $T_a(t) = T_0 + \delta \sin(\omega t)$ and $dT_a/dt = \delta\omega \cos(\omega t)$, which can be used as before in Eqs. (7a) and (7b) to solve for the feedforward output, giving

$$I_{FF}(t) = \frac{\delta\omega}{\rho}\left(1 + \frac{2\kappa_w}{\kappa_a}\right)\cos(\omega t) + \frac{\delta\kappa_w}{\rho}\left(1 - \frac{\omega^2\kappa_w}{\kappa_a}\right) \times \sin(\omega t) + \frac{\kappa_w}{\rho}(T_0 - T_b). \quad (15)$$

The setpoint for the feedback loop is given by $T_{SP}(t) = T_0 + \delta \sin[\omega(t - \tau_d)]$, which includes a phase lag of $\phi = \omega\tau_d$ with respect to $T_a(t)$. Since the edge of the adsorbent follows the ideal temperature program $T_a(t)$ as the center follows $T_{SP}(t)$, the phase lag between them produces a spatial variation of the temperature within the adsorbent. One must be particularly careful when using this approach to investigate reaction kinetics, since errors will result when data are analyzed with the assumption that the temperature of the entire adsorbent modulates uniformly. For this reason, the maximum useful modulation frequency is effectively limited to $\omega \ll \tau_d^{-1}$.

IV. ISOTHERMAL DESORPTION OF CO FROM Ni(110)

The desorption of CO from Ni(110) provides an ideal example for analysis with the step-TPD technique, since high-quality ramp-TPD data for this system and traditional analyses of them are readily available for comparison.[19,20] Our goal is to determine if new insight relevant to the desorption mechanism and energetics can be obtained by examining the functional dependence of the desorption rate on coverage at constant temperature. An exhaustive analysis of adsorption and desorption rate data for all coverages has been reported separately;[13] we will only "highlight" some results here to demonstrate the efficacy of the isothermal data collection and analysis.

Ramp-TPD data for this system show two peaks, one at ~360 K associated with conversion of the saturation (2 × 1) overlayer with a coverage near 1.0 ml to a $c(4\times2)$ overlayer with a coverage of 0.75 ml, and a second at ~440 K associated with sequential desorption from the $c(4\times2)$ structure and a structure with a coverage of 0.625 ml that shows $c(8\times2)$ symmetry at low temperature.[19,21] An analysis of TPD peak shapes by heating rate variation shows the apparent activation energy for desorption roughly constant near 31 kcal/mol for coverages below about 0.7 ml, then dropping to 26 kcal/mol as saturation is approached and the (2 × 1) overlayer forms.[20] The preexponential factor increases from $4\times10^{14}\ s^{-1}$ at low coverage to $2\times10^{15}\ s^{-1}$ near $\vartheta = 0.7$ ml, then drops for higher coverages in a compensatory manner as the activation energy decreases. The authors of Ref. 20 compared their data to several kinetic models involving lateral interactions and mobile precursor states, but were unable to draw detailed conclusions about the desorption mechanism.

Figure 5 shows the results of a typical step-TPD measurement. The solid line is the desorption rate and the dotted line is the temperature, both as functions of time. The surface was saturated with CO at $T = 80$ K, ramped to $T = 200$ K and held there for 30 s to anneal the overlayer prior to desorption, then ramped to the temperature at which the step program started, $T = 263$ K in this case. Note that the temperature program includes two steps—one to $T = 343$ K to collect data corresponding to the low-temperature peak observed in ramp-TPD measurements, and a second to $T = 423$ K to collect data corresponding to the high-temperature peak.[13,19,20] Also evident in Fig. 5 is a rapid ramp at the end of the temperature program to desorb any CO remaining on the surface. Since the desorption rate is $-d\vartheta/dt$, integration of the signal intensity from $t \to \infty$ to any point on the time axis allows the rate as a function of coverage to be determined for the regions where the temperature is constant. For the purposes of this discussion, we have assumed that the saturation coverage is 0.92 ml when performing the integration, as has been determined for this system from nuclear reaction analysis.[22]

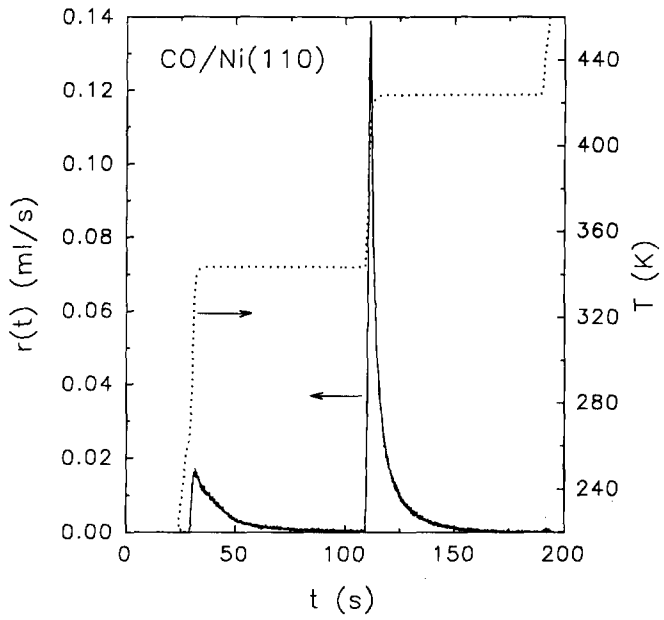

FIG. 5. Desorption rate vs time for a typical two-step TPD measurement of CO desorption from Ni(110).

For the ensuing discussion we will focus on the regime below $\vartheta = 0.6$ ml, where the adsorption probability is constant[13] and a $c(8\times2)$ overlayer with a saturation coverage of 0.625 ml is observed in LEED measurements at low temperature.[21] This range is included in the rate curve at the right of Fig. 5. Figure 6 shows curves of the desorption rate $r(\vartheta)$ as a function of ϑ for temperatures between 399 and 423 K, obtained by integrating the isothermal rate data with respect to time. Notice that straight lines, as would be expected for simple first-order kinetics with coverage-independent rate parameters, are not observed,

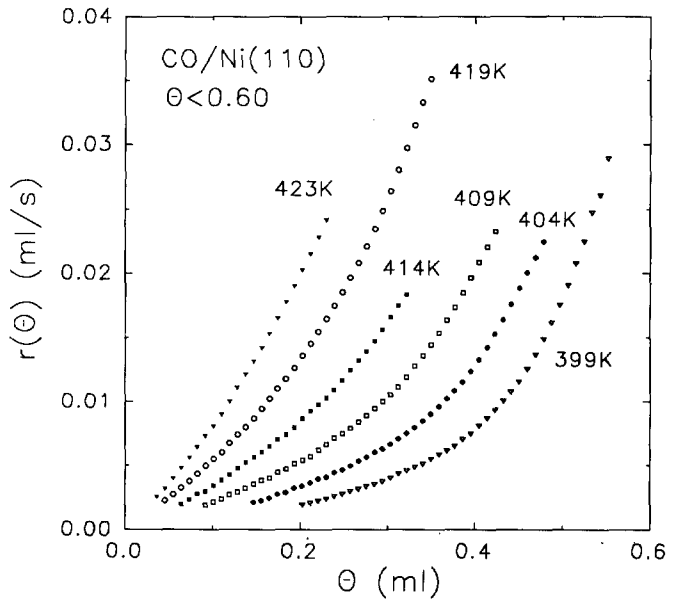

FIG. 6. Data like those at the right of Fig. 5 for $\vartheta < 0.6$ ml and the indicated temperatures, converted to $r(\vartheta)$ vs ϑ by integration of the measured rate with respect to time.

but instead the dependence of the rate on coverage at constant coverage appears to be stronger than first order.[23] We will show that a first-order model with coverage-independent rate parameters, modified to include a mobile precursor state as suggested by the constancy of the adsorption probability in this coverage range, accounts quantitatively for the temperature-dependent curvature in the data of Fig. 6.

Here we postulate an adsorption/desorption mechanism and develop the rate expression it predicts. This treatment is similar, though not identical, to others presented previously.[24] Assume first that a gas-phase CO molecule striking the surface is not directly chemisorbed at a site on the surface, but instead is temporarily "trapped" and held by weak dispersion forces in a precursor state, moving parallel to the surface until it either returns again to the gas phase or finds an open site at which it may chemisorb. Assume also that all chemisorbed molecules are effectively identical, and each has the adsorption environment characteristic of the complete overlayer eventually formed, in this case a lattice gas that shows $c(8\times2)$ order at low temperature. Each chemisorbed molecule occupies an area equivalent to $1/\vartheta_s$ surface sites, where ϑ_s is the ideal saturation coverage of the overlayer, since the surface is uniformly covered when this coverage is attained. Then the fraction of the surface sites available for chemisorption is $f = 1 - \vartheta/\vartheta_s$, where ϑ is the prevailing coverage in the chemisorbed state. In desorption the process is reversed: a chemisorbed molecule is thermally excited to the mobile precursor state, after which it either returns to an open area on the surface to chemisorb again or escapes to the gas phase. The potential well that binds the precursor molecules to the surface is only a few kcal/mol deep, so their coverage ϑ_p approaches zero, and $d\vartheta_p/dt = 0$. With this simplification, the mass balance for chemisorbed molecules is

$$\frac{d\vartheta}{dt} = \frac{\tau F k_{pc}(1 - \vartheta/\vartheta_s) - k_{cp}k_{pg}\vartheta}{k_{pg} + k_{pc}(1 - \vartheta/\vartheta_s)}. \tag{16}$$

In this expression F is the flux of molecules striking the surface, τ is the probability that an impinging molecule is trapped in the precursor state, and k_{ij} is the rate constant for conversion from state i to j, with c = chemisorbed, p = precursor, and g = gas. Two limiting behaviors can be identified. When $k_{pg} \gg k_{pc}$, equilibrium between the precursor state and the gas phase is approached during adsorption, the adsorption rate decreases linearly with coverage, and the desorption rate increases linearly with coverage. When $k_{pc} \gg k_{pg}$, the adsorption rate is independent of coverage, equilibrium between the chemisorbed and precursor states is approached during desorption, and the increase of the desorption rate with coverage is more rapid than linear. The adsorption/desorption behavior of CO on Ni(110) in this coverage range is consistent with the second case,[13] and it is this kinetic model to which we make a detailed comparison.

For conditions relevant to the step-TPD measurements, no adsorption occurs, and with $k_{pc} \gg k_{pg}$ the desorption rate $r = -d\vartheta/dt$ reduces to

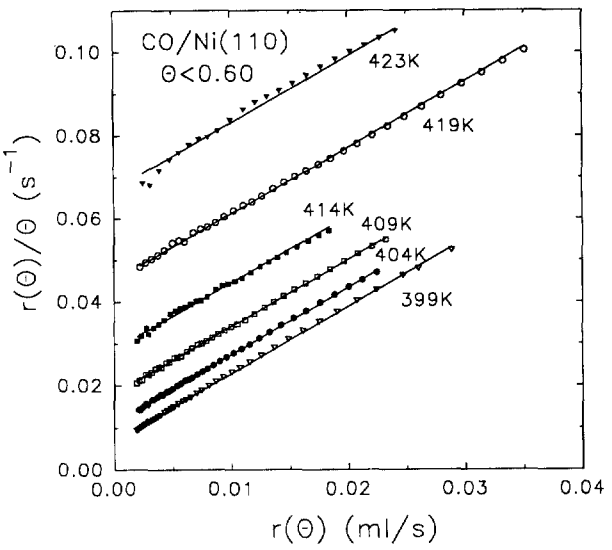

FIG. 7. The data of Fig. 6 arranged according to the form of Eq. (18). The equal slopes of the lines give $\vartheta_s = 0.63 \pm 0.02$ ml as an estimate for the saturation coverage of the overlayer, in excellent agreement with the coverage expected for the ideal $c(8\times2)$ overlayer evident in low temperature LEED measurements for this system.

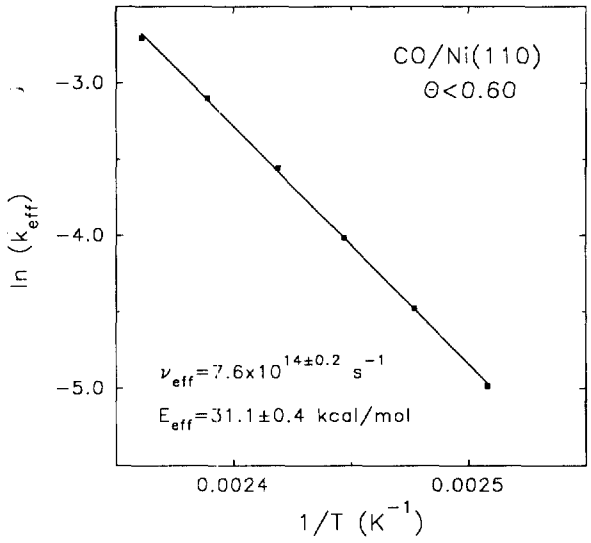

FIG. 8. An Arrhenius plot of the intercepts from Fig. 7. The combined activation energy is $E_{\text{eff}} = E_{cp} + E_{pg} - E_{pc} = 31.1 \pm 0.4$ kcal/mol, and the combined preexponential factor is $\nu_{\text{eff}} = \nu_{cp}\nu_{pg}/\nu_{pc} = 7.6\times10^{14\pm0.2}$ s^{-1}.

$$r = -\frac{k_{\text{eff}}\vartheta}{(1-\vartheta/\vartheta_s)}, \tag{17}$$

where $k_{\text{eff}} = k_{cp}k_{pg}/k_{pc}$. This expression can be rearranged to read

$$\frac{r}{\vartheta} = \frac{r}{\vartheta_s} - k_{\text{eff}}. \tag{18}$$

Thus if Eq. (16) and the associated assumptions reflect a true description of the adsorption/desorption mechanism, isothermal plots of r/ϑ vs r will yield straight lines with intercepts $k_{\text{eff}}(T)$ and equal slopes $1/\vartheta_s$. Plots of the $r(\vartheta)$ data according to this prescription are shown in Fig. 7. The collinearity of the points at each temperature is excellent, supporting the accuracy of this interpretation. With the assumption that the saturation coverage at the beginning of the measurements is 0.92 ml[20], the common slope of all the straight lines is $\vartheta_s = 0.63 \pm 0.02$ ml, in excellent agreement with the saturation coverage of an ideal $c(8\times2)$ overlayer on this surface.

Figure 8 shows an Arrhenius plot constructed from the intercepts of Fig. 7. From the slope of the Arrhenius plot one obtains $E_{\text{eff}} = E_{cp} + E_{pg} - E_{pc} = 31.1 \pm 0.4$ kcal/mol for the effective activation energy, and from the intercept $\nu_{\text{eff}} = \nu_{cp}\nu_{pg}/\nu_{pc} = 7.6\times10^{14\pm0.2}$ s^{-1} for the effective preexponential factor. The precision of these numbers is unusually high because the algebraic form of the rate function has been properly identified from the curves of $r(\vartheta)$ vs ϑ, so that all the data in Figs. 6 and 7 contribute to the determination of only three parameters — ϑ_s, E_{eff}, and ν_{eff}. A comparison to the predictions of transition state theory indicates that the magnitude of ν_{eff} is consistent with the assignment of free two-dimensional rotation and translation to the transition state leaving the precursor well and six vibrational degrees of freedom to the chemisorbed state. Since E_{eff} measures the net difference in energy between the chemisorption state and the gas phase, it can be identified as the negative of the heat of adsorption for CO molecules in this coverage range.[13]

V. SUMMARY AND CONCLUSIONS

We have described a computer-based feedforward/feedback scheme for control of the temperature of a resistively heated metal adsorbent in UHV. The feedforward controller is based on a second-order model of the system's response, modified to account for the time required for heat to conduct from the input points at the adsorbent's edges to the temperature measurement point at its center. The feedback controller includes proportional and derivative actions to compensate for load disturbances and inadequacies in the feedforward model. The use of the controller is demonstrated for the specific case of rapid step changes in temperature, which can be used to measure desorption rates under isothermal conditions.

The efficacy of the step-TPD approach is demonstrated for the particular case of CO desorption from Ni(110) for coverages below 0.6 monolayer, where a $c(8\times2)$ overlayer is observed in LEED measurements at low temperature. The variation of the rate with coverage at constant temperature identifies clearly the participation of a precursor state, and a detailed analysis based on this notion is consistent with the observed behavior of the adsorption probability at low temperature, and it provides a convincing mechanistic description of the desorption process. The rate parameters for the elementary steps in the desorption process are nearly independent of coverage, but the overall desorption rate shows nonlinear behavior attributable to the participation of the precursor state. The effective activation energy for desorption, $E_{\text{eff}} = 31.1$ kcal/mol, can be identified as the heat of adsorption in this circumstance,

and the magnitude of effective preexponential factor, $\nu_{\text{eff}} = 7.6\times10^{14}\ \text{s}^{-1}$, is consistent with free rotation and translation of molecules leaving the precursor state and six vibrational degrees of freedom for molecules in the chemisorbed state. In principle, the information necessary to draw these detailed conclusions was available in the numerous ramp-TPD studies of this system reported previously. In practice, however, we find that mechanistic features of the desorption process are more clearly evidenced in isothermal $r(\vartheta)$ vs ϑ data derived from step-TPD measurements.

ACKNOWLEDGMENTS

We acknowledge gratefully the support of this work by the Shell Oil Company Foundation and by the National Science Foundation on Contract Nos. CBT-8808655 and DMR-8818558 (Cornell Materials Science Center).

APPENDIX

Here we present the solution to Eqs. (7a) and (7b) for a feedforward controller output like that shown in Fig. 4, which produces a rapid change in temperature from $T_1 = T_b + \rho I_1/\kappa_w$ for $t<0$ to $T_2 = T_b + \rho I_2/\kappa_w$ for $t\to\infty$. When calculating I_1 and I_2 corresponding to temperatures T_1 and T_2, values of κ_w/ρ determined from steady-state measurements should be used.

First, let $\lambda = \kappa_a/2\kappa_w$. Equations (7a) and (7b) can be combined to give a single, second-order differential equation for $T_a(t)$:

$$\frac{d^2T_a}{dt^2} + 2\kappa_w(1+\lambda)\frac{dT_a}{dt} + 2\kappa_w^2\lambda(T_a - T_b) = 2\kappa_w\lambda\rho I(t). \tag{A1}$$

The roots of the characteristic equation are

$$r_+, r_- = \kappa_w[\pm(1+\lambda^2)^{1/2} - (1+\lambda)]. \tag{A2}$$

The solution to Eq. (A1) for this circumstance is:

$$\text{For } t<0,\quad I(t) = I_1 \quad\text{and}\quad T_a(t) = T_1. \tag{A3}$$

For $0<t<\tau_0$, $I(t) = 1$, and

$$T_a(t) = \frac{\rho}{\kappa_w} + T_b + \frac{\rho - \kappa_w(T_1 - T_b)}{2\kappa_w^2(1+\lambda^2)^{1/2}} \times [r_- \exp(r_+ t) - r_+ \exp(r_- t)]. \tag{A4}$$

For $t>\tau_0$, $I(t) = I_2$, and

$$T_a(t) = T_2 + \frac{\rho - \kappa_w(T_1 - T_b)}{2\kappa_w^2(1+\lambda^2)^{1/2}} \times [r_- \exp(r_+ t) - r_+ \exp(r_- t)] - \frac{\rho - \kappa_w(T_2 - T_b)}{2\kappa_w^2(1+\lambda^2)^{1/2}} \{r_- \exp[r_+(t-\tau_0)] - r_+ \exp[r_-(t-\tau_0)]\}. \tag{A5}$$

In these expressions the values of κ_w and ρ are those appropriate for rapid heating. The setpoint input to the feedback loop is the time-delayed form of this solution, which is given by $T_{\text{SP}}(t) = T_a(t-\tau_d)$. The on-time τ_0 for maximum feedforward output is chosen to make $T_a(t)$ reach its steady-state value T_2 as quickly as possible without overshoot. One can show from Eq. (A5) that the optimum choice for τ_0 is given by

$$\tau_0 = \frac{1}{r_+}\ln\left(\frac{\rho - \kappa_w(T_2 - T_b)}{\rho - \kappa_w(T_1 - T_b)}\right). \tag{A6}$$

[1] D. A. King, Surf. Sci. **47**, 384 (1975); J. L. Falconer and J. A. Schwarz, Cat. Rev.-Sci. Eng. **25**, 141 (1983).
[2] P. A. Redhead, Vacuum **12**, 203 (1962).
[3] Techniques for ramp-TPD analysis are summarized and compared in: A. M. de Jong and J. W. Niemantsverdriet, Surf. Sci. **223**, 355 (1990).
[4] This fact is the basis for "threshold" analysis of ramp-TPD spectra. E. Habenschaden and J. Küppers, Surf. Sci. **138**, L147 (1984); J. B. Miller, H. R. Siddiqui, S. M. Gates, J. N. Russell, Jr., J. T. Yates, Jr., J. C. Tully, and M. J. Cardillo, J. Chem. Phys. **87**, 6725 (1987).
[5] J. M. Soler and N. Garcia, Surf. Sci. **124**, 563 (1983).
[6] R. Gorte and L. D. Schmidt, Appl. Surf. Sci. **3**, 381 (1979).
[7] R. N. Carter and A. B. Anton, J. Vac. Sci. Technol. A **10**, 344 (1992).
[8] F. Kreith and M. S. Bohn, *Principles of Heat Transfer*, 4th ed. (Harper and Row, New York, 1986).
[9] A. A. Frost and R. G. Pearson, *Kinetics and Mechanism* (Wiley, New York, 1961).
[10] A. B. Anton and D. C. Cadogan, Surf. Sci. **239**, L548 (1990).
[11] T. H. Ellis, M. Morin, L. H. DuBois, M. J. Cardillo, and S. D. Kevan, in *Kinetics of Interface Reactions*, edited by M. Grunze and H. J. Kreuzer (Springer, Heidelberg, 1987), pp. 63–70.
[12] C. Kohrt and R. Gomer, J. Chem. Phys. **52**, 3283 (1970); H. A. Engelhardt and D. Menzel, Surf. Sci. **57**, 591 (1976); M. A. Barteau, E. I. Ko, and R. J. Madix, *ibid.* **102**, 99 (1981); H. Michel, R. Opila, and R. Gomer, *ibid.* **105**, 48 (1981).
[13] M. A. DeAngelis, A. M. Glines, and A. B. Anton, J. Chem. Phys. **96**, 8582 (1992).
[14] A. M. Glines, R. N. Carter, and A. B. Anton, Rev. Sci. Instrum. **63**, 1826 (1992).
[15] D. E. Seeborg, T. F. Edgar, and D. A. Mellichamp, *Process Dynamics and Control* (Wiley, New York, 1989), Chaps. 17 and 18.
[16] J. R. Engstrom and W. H. Weinberg, Rev. Sci. Instrum. **55**, 404 (1984).
[17] Control strategies based on a dynamic feedforward model and a time-shifted setpoint to compensate for time delay are known as "Smith Predictors." O. J. M. Smith, Chem. Eng. Prog. **53**, 217 (1957).
[18] J. R. Engstrom and W. H. Weinberg, Surf. Sci. **201**, 145 (1988); J. Chem. Phys. **87**, 4211 (1987).
[19] B. A. Gurney and W. Ho, J. Vac. Sci. Technol. A **3**, 1541 (1985); M. D. Alvey, M. J. Dresser, and J. T. Yates, Jr., Surf. Sci. **165**, 447 (1986).
[20] C. S. Feigerle, S. R. Desai, and S. H. Overbury, J. Chem. Phys. **93**, 787 (1990).
[21] R. J. Behm, G. Ertl, and V. Penka, Surf. Sci. **160**, 387 (1985).
[22] P. R. Norton, P. E. Binder, and T. E. Jackman, Surf. Sci. **175**, 313 (1986).
[23] A complete analysis for all coverages reveals that the rate *is* a linear function of coverage at constant temperature for the desorption reaction that converts the overlayer from a (2×1) structure with a saturation coverage of $\vartheta = 1.0$ ml to a $c(4\times2)$ overlayer with a saturation coverage of 0.75 ml. This fact is also evident in the shape of the isothermal portion of the rate curve at the left of Fig. 5, which gives a straight line when plotted as $\ln[r(t)]$ vs t. The contrast of this behavior to that evident for lower coverages identifies a transition in the adsorption/desorption mechanism that plays a critical role in the evolution of the (2×1) and $c(4\times2)$ structures with temperature and coverage. See Ref. 13 for details.
[24] R. Gorte and L. D. Schmidt, Surf. Sci. **76**, 559 (1978); A. Cassuto and D. A. King, *ibid.* **102**, 388 (1981).